Saeedian, Meysam; Eskandari, Bahman; Rouzbehi, Kumars; Taheri, Shamsodin; Pouresmaeil, Edris

Employing Virtual Synchronous Generator with a New Control Technique for Grid Frequency Stabilization

Published in:
Proceedings of the 22nd European Conference on Power Electronics and Applications, EPE'20 ECCE Europe

DOI:
10.23919/EPE20ECCEEurope43536.2020.9215605

Published: 01/01/2020

Document Version
Peer-reviewed accepted author manuscript, also known as Final accepted manuscript or Post-print

Please cite the original version:
Saeedian, M., Eskandari, B., Rouzbehi, K., Taheri, S., & Pouresmaeil, E. (2020). Employing Virtual Synchronous Generator with a New Control Technique for Grid Frequency Stabilization. In *Proceedings of the 22nd European Conference on Power Electronics and Applications, EPE'20 ECCE Europe* Article 9215605 (European Conference on Power Electronics and Applications). IEEE.
https://doi.org/10.23919/EPE20ECCEEurope43536.2020.9215605

Employing Virtual Synchronous Generator with a New Control Technique for Grid Frequency Stabilization

Meysam Saeedian[1], Bahman Eskandari[1], Kumars Rouzbehi[2], Shamsodin Taheri[3], Edris Pouresmaeil[1]
[1] Department of Electrical Engineering and Automation, Aalto University, 02150 Espoo, Finland
[2] Department of Electrical Engineering, University of Seville, Seville, Spain
[3] Department of Computer Science and Engineering, Université du Québec en Outaouais, 101 Rue Saint-Jean-Bosco, QC J8X 3X7, Gatineau, Canada

Keywords

«Virtual synchronous generator», « Inertia emulation», «Grid frequency stability», «Grid-connected voltage source converter».

Abstract

This paper aims to develop a control technique for grid-interfaced voltage source converters in distributed power generation systems. The proposed method is composed of two control loops, i.e., inner and outer controllers. The former one is based on a fast current control technique, with the capability of handling active and reactive power. The inertial characteristic of conventional synchronous generators is mimicked by means of the outer control loop, with the aim of providing required inertia for the main grid. This developed control strategy results in mitigation of frequency nadir and rate of change of frequency level in the system frequency response, and thereby, frequency stability during disturbances. Herein, the dynamics of the suggested control scheme is first presented in the *dq* rotating frame for the design of current control loops. Virtual inertia emulation using the frequency-power response based topology is then discussed in detail. Finally, a 200 kVA virtual synchronous generator is simulated in MATLAB to support theoretical analyses and demonstrate the appropriate performance of the suggested technique in control of interfaced voltage source converters between distributed energy sources and power grids.

I. Introduction

Power systems dominated by conventional synchronous generators (SGs) are robust against severe voltage/frequency deviations caused by ever-changing demand and generation profiles [1, 2]. This is because SGs can inject preserved kinetic energy (and thereby rotating inertia and damping properties) in their rotating mass to the main network during contingencies [3]. Nonetheless, the interconnection of renewable energy sources (RESs) with main grids is steadily increasing due to the environmentally friendly perspectives and ever-increasing demand for electricity [4]. For example, the government of Japan aims to connect photovoltaic power plants with 14.3 GW and 53 GW power to its power system by 2020 and 2030, respectively [5]. In such systems (i.e., RESs), voltage source converters (VSCs) act as the interface media with the utility which have neither actual rotor nor damping property. The most challenging issue with the high-level penetration of RESs to the grid is lack of inertia, which gives rise to the excessive rate of change of frequency (RoCoF) and maximum frequency deviation in respect of reference value (i.e., frequency nadir), as illustrated in Fig. 1 [6, 7]. This undesirable condition may yield to pole slipping and catastrophic failure of generating units. Pole slipping occurs if *df/dt* rate is between 1.5 Hz/sec and 2 Hz/sec [1].

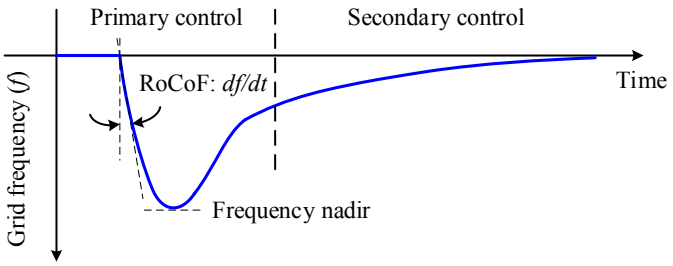

Fig. 1: Grid frequency deviations following a step-up change in demand.

To mitigate the RoCoF level and improve frequency stability, the idea of providing additional inertia by means of virtual synchronous generator (VSG) can be implemented [1, 8]. This concept was presented by Beck and Hesse in 2007 [9], which is based on emulating dynamic characteristics of real SGs by power-electronic based generators. In other words, frequency regulation/restoration is obtained by the grid-tied VSC active power control. The issues related to the lack of inertia in power grids with large-scale integration of RESs have been addressed in numerous papers. For instance, [10] proposed the method of supplying virtual inertia by the dc-link voltage controller of VSCs. In [11], the authors reported power synchronization control (PSC) of grid-tied VSCs, which uses the inner synchronization mechanism of ac systems. A simplified model of a conventional SG has been presented in [12] to generate current references for the hysteresis controller of a grid-connected VSC. A detailed-nonlinear model of VSG implementation has been derived in [13]. Moreover, a new technique of providing virtual inertia titled "synchronverter" was proposed in [14]. The VSG model introduced in [8] has been designed to integrate energy storage systems (ESSs) to the microgrid. Furthermore, the influence of VSG system on the dynamic performance of microgrids has been discussed in [15]. In [16], the authors compared the transient response of the VSG and traditional droop control. It should be emphasized that an advantage of VSGs compared to the real SGs is that we can select the parameters of its dynamic equation in real-time, which can provide faster and better frequency stability during the grid disturbances.

The contribution of this paper is to develop a control technique for grid-interfaced VSCs, which comprises two control loops. High-quality active and reactive power can be delivered to the main grid through the inner controller. On the other hand, the inertial response characteristic of the real SGs is emulated by the outer control loop. Consequently, it provides virtual inertia and grid frequency stabilization in power grids under high integration of RESs. The remainder of this work is presented as follows: Section II presents the structure of VSC system and proposed control technique. Furthermore, the frequency-power response based virtual inertia topology is discussed in Section II. The appropriate performance of the control method is confirmed by the simulation results provided in Section III. Finally, conclusions are presented in Section IV.

II. Proposed Control Scheme

Fig. 2 demonstrates the schematic diagram of a grid-tied VSC system, comprising of a three-phase two-level converter, an interfacing L or LC filter, which blocks high-frequency current harmonics generated by the VSC from entering to the main grid. The balanced power grid is modeled as a Thevenin equivalent circuit with the input impedance of R_G and L_G. Photovoltaic panels, wind turbines or storage devices can be applied as the primary source of the VSC (i.e., v_{in}). As the focus of this work is on the VSC control technique, the design and control of primary energy storage are out of the scope of this paper. Moreover, v_{tabc}, v_{abc} and u_{abc} denote the three-phase voltage vectors of the VSC terminal, point of common coupling (PCC), and main grid, respectively.

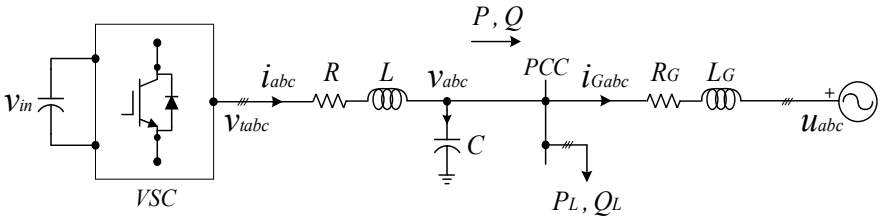

Fig. 2: Circuit diagram of the grid-tied VSC.

A. Dynamic Study of the Proposed Technique

Generally, the ac-side of VSCs can be considered as a three-phase ac voltage source [2]. According to Fig. 2 and neglecting filter capacitor current (i_C), the as-side dynamics of the grid-connected VSC is presented as follow:

$$L\frac{di_{abc}}{dt} = -Ri_{abc} + v_{tabc} - v_{abc} \tag{1}$$

where i_{abc} stands for the VSC output current vector. Considering balance operation of the power network, the output voltage and current of the VSC can be represented in the dq frame by following Park transformation:

$$T_{abc/dq} = \frac{2}{3}\begin{bmatrix} \cos\theta & \cos\left(\theta - 2\pi/3\right) & \cos\left(\theta + 2\pi/3\right) \\ -\sin\theta & -\sin\left(\theta - 2\pi/3\right) & -\sin\left(\theta + 2\pi/3\right) \end{bmatrix} \tag{2}$$

$$L\frac{di_d}{dt} = -Ri_d + \omega Li_q + v_{td} - v_d \tag{3}$$

$$L\frac{di_q}{dt} = -\omega Li_d - Ri_q + v_{tq} - v_q \tag{4}$$

where ω denotes the angular frequency of the grid and can be obtained by a phase-locked loop (PLL) connected to the PCC. When the d-axis of dq frame aligns with the grid voltage, the q-axis component of voltage vector at the PCC becomes equal to zero (i.e., v_q=0). In this case, the injected instantaneous active and reactive power from the VSC to the PCC are obtained as follows:

$$P(t) = \frac{3}{2}v_d i_d \tag{5}$$

$$Q(t) = -\frac{3}{2}v_d i_q. \tag{6}$$

Thereby, the dq-components of the command current vector can be calculated by:

$$i_d^* = \frac{2P^*}{3v_d} \tag{7}$$

$$i_q^* = -\frac{2Q^*}{3v_d}. \tag{8}$$

B. Inner Control Loop

To achieve a fast and accurate active/reactive power injection, the dq-components of the current vector (i_d and i_q) should be controlled in two separate and independent control loops. Defining $\lambda_{dq}=L(di_{dq}/dt)+Ri_{dq}$ and substituting in (3) and (4), the output voltage vector of the VSC can be represented by:

$$v_{td} = \lambda_d - L\omega i_q + v_d \tag{9}$$

$$v_{tq} = \lambda_q + L\omega i_d. \tag{10}$$

As demonstrated in (9) and (10), the cross-coupling terms (i.e., $L\omega i_d$ and $L\omega i_q$) emerge in the dq current control loops. The interdependency of injected active and reactive power is attenuated by adding decoupling terms of $L^*\omega i_d$ and $L^*\omega i_q$ to the dq-axes current loops as depicted in Fig. 3. The terms L^* and v_d^* denote the estimated values for interfacing inductance and PCC voltage, respectively. It should be emphasized that i_d and i_q are controlled through simple proportional-integral (PI) controllers since grid frequency components are seen as dc components in the park-transformed variables during the steady-state condition. The transfer function of PI controllers is given by:

$$\frac{\lambda_d(s)}{\Delta i_d(s)} = \frac{\lambda_q(s)}{\Delta i_q(s)} = k_p + \frac{k_i}{s} \tag{11}$$

in which k_p (k_i) is proportional (integral) gain and Δi_{dq} denotes the difference between the actual output current and reference current of the VSC (i.e., $\Delta i_{dq}=i_{dq}^*-i_{dq}$). After simplification, the transfer function of the inner control loops are determined by (12):

$$\frac{i_d(s)}{i_d^*(s)} = \frac{i_q(s)}{i_q^*(s)} = \frac{k_p}{L} \frac{s + \frac{k_i}{k_p}}{s^2 + \left(\frac{R + k_p}{L}\right)s + \frac{k_i}{L}}. \tag{12}$$

It is clear that the zero at $-k_i/k_p$ will affect the dynamic response of the VSC. This effect can be mitigated by applying a low-pass filter in the current control loops (see Fig. 4). Consequently, the transfer function of the system is identical to a second-order transfer function $\omega_n^2/(s^2+2\zeta\omega_n s+\omega_n^2)$, in which k_i and k_p parameters are designed by (13) and (14).

$$k_p = 2L\zeta\omega_n - R \tag{13}$$

$$k_i = L\omega_n^2 \tag{14}$$

where ζ and ω_n denote the damping factor and natural undamped angular frequency of transfer function, respectively.

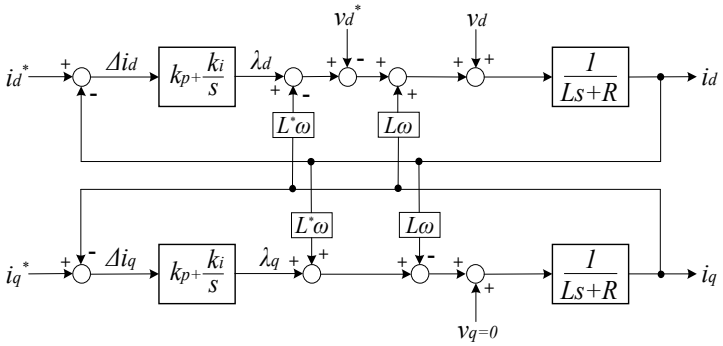

Fig. 3: Inner control loop.

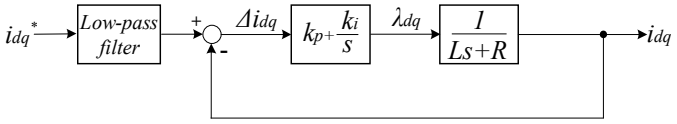

Fig. 4: Simplified inner control loops.

C. Grid Frequency Support

As mentioned in Section I, the imbalance between generation and demand in power grid dominated by high-penetration of RESs leads to the frequency deviations and drastic RoCoF level. This mismatch can be represented by the following swing equation [3]:

$$P_G - P_L = \frac{1}{2}\frac{d\left(J\omega^2\right)}{dt} \tag{15}$$

where P_G, P_L, J, and ω stand for the generated power, demanded power, moment of inertia of the turbine-generator couple, and system angular frequency, respectively. Equation (15) can be represented based on the inertia constant (H), which is defined as kinetic energy over the SG apparent power S_G [17]:

$$H = \frac{J\omega^2}{2S_G}. \tag{16}$$

Followed by simplification, (15) can be written as:

$$\frac{2H}{f}\frac{df}{dt} = \frac{P_G - P_L}{S_G} \tag{17}$$

In this equation, df/dt is the RoCoF of the system, which must be restricted. The frequency deviation is more severe if a major portion of the demanded power is provided by power electronic-based generators. To mitigate the perturbation, the inertial response characteristic of the conventional SG should be emulated by the VSC. Various techniques have been introduced in the literature for adding virtual inertia into the grid, which are classified in Fig. 5 [17]. It should be highlighted that the main concept of such topologies is the same, however, the implementation is different depending on the application. Herein, modified frequency-power response based topology is applied for the VSG system (Fig. 6):

$$P_{VSG} = \frac{M}{1 + sT_{VSG}} s\omega + D\Delta\omega \tag{18}$$

where $\Delta\omega$ denotes the difference between reference angular frequency and grid angular frequency, and T_{VSG} is the time constant of the added low-pass filter. The term M is virtual inertia coefficient that mitigates the RoCoF level by providing a fast dynamic frequency response. Moreover, the reduction of frequency nadir is fulfilled by damping power coefficient D. These two parameters can be calculated by [18]:

$$M = \frac{P_{VSC}}{\left(\frac{df}{dt}\right)_{\max}} \tag{19}$$

$$D = \frac{P_{VSC}}{(\Delta f)_{\max}} \tag{20}$$

where P_{VSC} is the nominal power rating of the grid-interfaced VSC, $(df/dt)_{max}$ is maximum acceptable RoCoF and $(\Delta f)_{max}$ is the maximum acceptable frequency deviation. It should be emphasized that when the grid frequency falls (raises), the RoCoF is negative (positive). Thereby, M must be selected negative to inject (absorb) active power during load increment (decrement). The overall schematic diagram of the proposed control technique is depicted in Fig. 7.

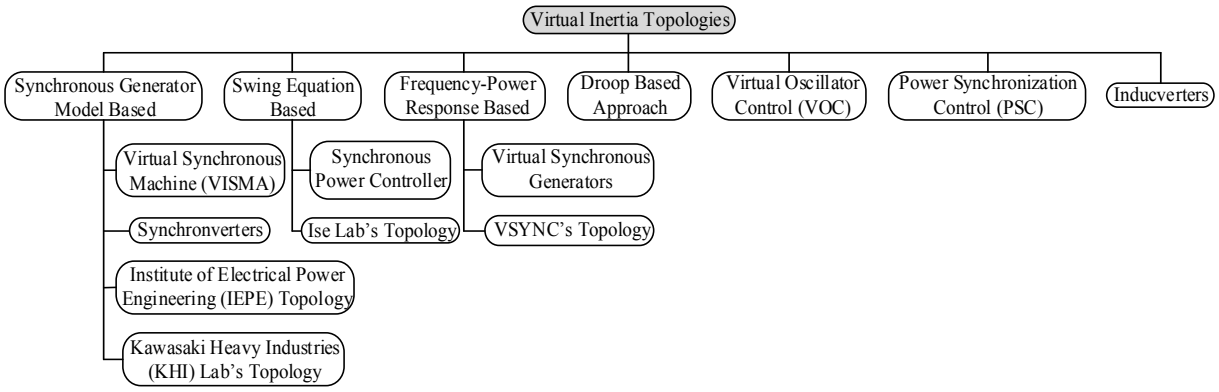

Fig. 5: Classification of virtual inertia topologies.

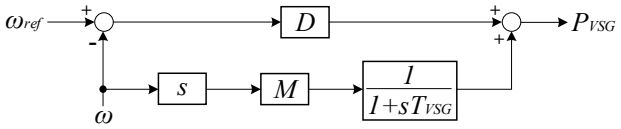

Fig. 6: Modified frequency-power response based technique for implementing virtual inertia.

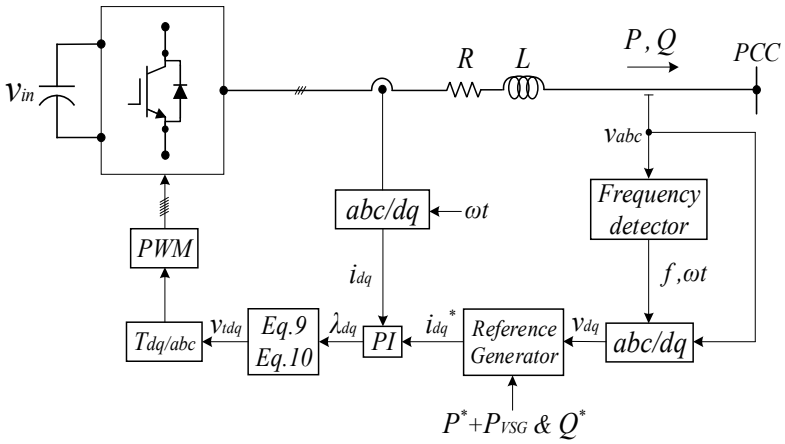

Fig. 7: Overall diagram of the presented control scheme.

III. Simulation Results

To confirm the effectiveness and improve the primary frequency restoration by the proposed control technique, a detailed model of the understudy system (Fig. 7) is implemented in Matlab. Table I summarizes the main parameters of the model in Fig. 7. It should be noted that a 2 MVA synchronous generator is replaced with the main grid to analyze the dynamic characteristics of the implemented model. The system is tested under sudden and large perturbations, and the results are presented as follows. The operation of the system with and without adding virtual inertia is then illustrated and compared.

Table I: Specifications of the SG and VSC in the Simulated Model

Parameter	Value
SG nominal apparent power	2 MVA
SG nominal voltage (line-to-line)	400 V_{RMS}
Inertia constant	2.78 s
Nominal frequency	50 Hz
VSC nominal power	200 kVA
VSC switching frequency	5 kHz
DC-link voltage	750 V
Filter size	L=1.5 mH and R=1 mΩ
Local load demand	500±50 kW

A. Sudden Increment in the Load

In this scenario, a step-up change in the load is considered. In the steady-state operating condition, the grid-tied VSC provides 40% of the power demanded by the local load (500 kW). Moreover, the second frequency regulation is provided by the simulated SG. An additional load with the power of 50 kW is added to the first load at t=10 sec. Then, the grid frequency is measured with/without virtual inertia provided by the outer control loop. The obtained results are brought in Fig. 8(a). As can be observed from this figure, the grid frequency drops to 49.88 Hz after disturbance and restored to the nominal value (50 Hz) after a short period. When the outer controller is taken into account, the frequency nadir reaches 49.96 Hz and the grid frequency is stabilized after 3 seconds. Thereby, the dynamic performance of the grid frequency (RoCoF level and frequency nadir) is improved by adding virtual inertia to the grid. The VSC output power is also demonstrated in Fig. 8(b). As observed from this figure, the VSC output power steadily raises to 240 kW during the disturbance. It should be emphasized that the additional injected power by VSC is proportional to how much frequency support is required.

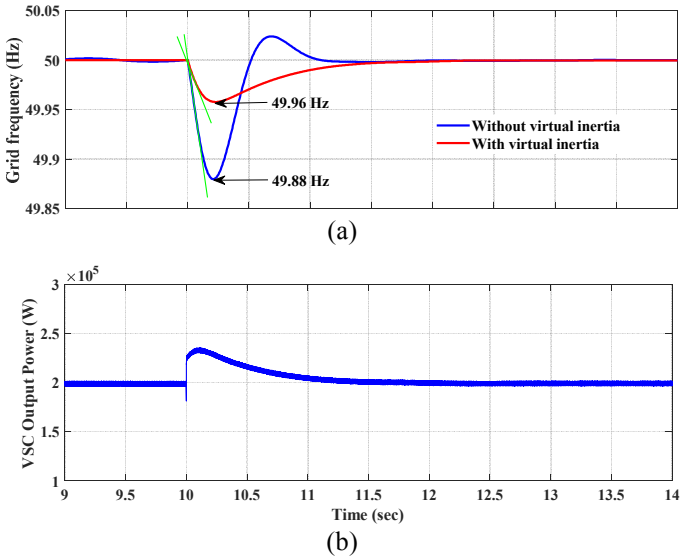

Fig. 8: (a) Grid frequency and (b) VSC output power curves under step-up change in the demand.

B. Sudden Decrement in the Load

The grid frequency and VSC output power are also measured during step-down change in the demand. The obtained results can be seen in Fig. 9. It is clear that the maximum frequency deviation is decreased from 0.12 Hz to 0.04 Hz when the power is absorbed by VSC at t=10 sec. Furthermore, the RoCoF level is mitigated by the additional inertia provided by the outer controller (Fig. 9(a)). These simulation results validate the feasibility and suitable performance of the presented control technique under sudden increment and decrement of the demand.

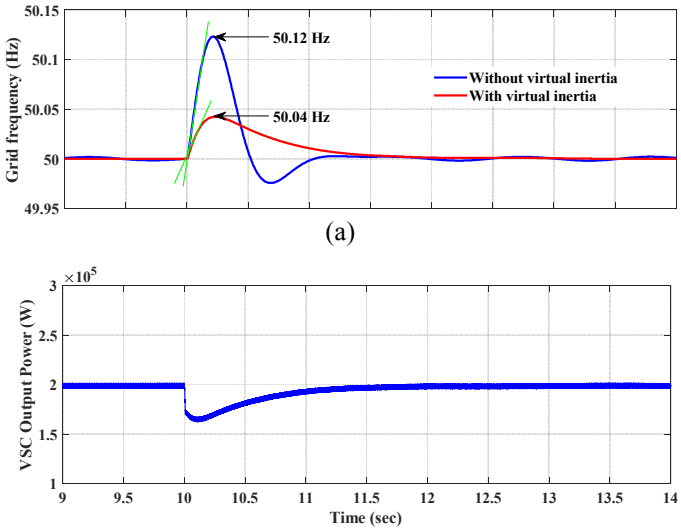

Fig. 9: (a) Grid frequency and (b) VSC output power curves under step-down change in the demand.

IV. Conclusions

Herein, a developed control technique for grid-interfaced VSCs has been presented. The proposed scheme comprises inner and outer control loops. The former one is based on a fast current controller, by which high-quality active and reactive power is delivered to the main network. The outer control loop provides frequency support during disturbances by mimicking the dynamics of conventional synchronous machines. Thereby, the maximum frequency deviation and RoCoF level can be mitigated. The mathematical structure of the proposed controller has been presented in detail. Finally, the feasibility and proper performance of the presented controller has been confirmed by simulation results obtained from a 200 kVA VSG model.

References

[1] Fang J., Li H., Tang Y., and Blaabjerg F.: On the Inertia of Future More-Electronics Power Systems, *IEEE Jour. Emerg. and Selec. Topics in Power Electron.*, vol. 7, no. 4, pp. 2130-2146, Dec. 2019.

[2] M. Saeedian, B. Eskandari, S. Taheri, M. Hinkkanen, and et al.: A Control Technique Based on Distributed Virtual Inertia for High Penetration of Renewable Energies Under Weak Grid Conditions, *IEEE Systems Journal*, doi: 10.1109/JSYST.2020.2997392.

[3] Alipoor J., Miura Y., and Ise T.: Power System Stabilization Using Virtual Synchronous Generator with Alternating Moment of Inertia, *IEEE Jour. Emerg. and Selec. Topics in Power Electron.*, vol. 3, no. 2, pp. 451-458, Jun. 2015.

[4] Sepehr A., Pouresmaeil E., Saeedian M., Routimo M., and et al.: Control of Grid-Tied Converters for Integration of Renewable Energy Sources into the Weak Grids, *Inter. Conf. on Smart Energy Systems and Technologies (SEST)*, Porto, Portugal, pp. 1-6, 2019.

[5] Bevrani H., Ise T., and Miura Y.: Virtual synchronous generators: A survey and new perspectives, *Int. Jour. Electrical Power and Energy Systems*, vol. 54, pp. 244-254, Jan. 2014.

[6] Hailin Z., Qiang Y., and Hongmei Z.: Multi-loop Virtual Synchronous Generator Control of Inverter-based DGs Under Microgrid Dynamics, *IET Generation, Transmission and Distribution*, vol. 11, no. 3, pp. 795-803, Feb. 2017.

[7] B. Pournazarian, E. Pouresmaeil, M. Saeedian, M. Lehtonen, and et al.: Microgrid Frequency & Voltage Adjustment Applying Virtual Synchronous Generator, *Inter. Conf. on Smart Energy Systems and Technologies (SEST)*, Porto, Portugal, pp. 1-6, 2019.

[8] Bose U., Chattopadhyay S. K., Chakraborty C., and Pal B.: A Novel Method of Frequency Regulation in Microgrid, *IEEE Trans. Ind. Appl.*, vol. 55, no. 1, pp. 111-121, Jan.-Feb. 2019.

[9] Beck H. P., and Hesse R.: Virtual synchronous machine, *Inter. Conf. Electrical Power Quality and Utilisation., Barcelona*, Spain, pp. 1-6, Oct. 2007.

[10] Fang J., Lin P., Li H., Yang Y., and et al.: An Improved Virtual Inertia Control for Three-Phase Voltage Source Converters Connected to a Weak Grid, *IEEE Trans. Power Electron*., vol. 34, no. 9, pp. 8660-8670, Sept. 2019.

[11] Zhang L., Harnefors L., and Nee H. P.: Power-Synchronization Control of Grid-Connected Voltage-Source Converters, *IEEE Trans. Power System*, vol. 25, no. 2, pp. 809-920, May. 2010.

[12] Hesse R., Turschner D., and Beck H. P.: Micro Grid Stabilization Using the Virtual Synchronous Machine (VISMA), *Inter. Conf. on Renewable Energies and Power Quality (ICREPQ'09)*, Valencia, Spain, pp. 1-6, Apr. 2009.

[13] Arco S. D., Suul J. A., and Fosso O. B.: A Virtual Synchronous Machine Implementation for Distributed Control of Power Converters in Smartgrids, *Elect. Power Syst. Res.*, vol. 122, pp. 180–197, May. 2015.

[14] Zhong Q. C., and Weiss G.: Synchronverters: Inverters that Mimic Synchronous Generators, *IEEE Trans. Ind. Electron.*, vol. 58, no. 4, pp. 1259–1267, Apr. 2011.

[15] Soni N., Doolla S., and Chandorkar M. C.: Improvement of Transient Response in Microgrids Using Virtual Inertia, *IEEE Trans. Power Del*., vol. 28, no. 3, pp. 1830–1838, Jul. 2013.

[16] Frack P. F., Doncker R. W. D., Mercado P. E., and Molina M. G.: Emulation of Synchronous Machine for Frequency Stability Improvement in Microgrids, *Inter. Conf. Power Electron. and Drive System*, Sydney, Australia, pp. 59–66, Jun. 2015.

[17] Tamrakar U., Shrestha D., Maharjan M., Bhattarai B. P., and et al.: Virtual Inertia: Current Trends and Future Directions, *Journal of Applied Sciences*, vol. 7, no. 7, pp. 1-29, Jun. 2017.

[18] Tamrakar U., Galipeau D., Tonkoski R., and Tamrakar I.: Improving transient stability of photovoltaic-hydro microgrids using virtual synchronous machines, *IEEE Eindhoven PowerTech*, Eindhoven, pp. 1-6, Jun. 2015.